Simultaneous Retreival of Surface Wind Speed and Rain Rate using Radar and Radiometer Measurements

Shannon T Brown and Christopher S Ruf

University of Michigan
Ann Arbor, MI USA
734-764-6561 (V), 734-936-0503 (F),
brownst@umich.edu / cruf@umich.edu (E)

Abstract – A retrieval algorithm has been developed which simultaneously estimates the over ocean near-surface wind speed and rain rate profile using data from a 10.7 GHz microwave radiometer and a dual-frequency Doppler radar. The algorithm uses the radar backscatter measurements to estimate two parameters of the gamma drop size distribution (GDSD) at each range gate. The parameterized GDSD can be integrated to determine the rain rate profile. The wind speed is estimated from the 10.7 GHz brightness temperatures (T_Bs) by removing the contribution from the atmosphere and isolating the contribution from the surface wind speed. The atmospheric optical depth at 10.7 GHz is estimated by integrating the extinction coefficient determined at each radar range gate using the parameterized GDSD and Mie theory. Results of wind speed and rain rate retrievals are presented from a field campaign in June of 2003 in which several precipitation overflights were made with a NASA DC-8 equipped with the PR-2 radar and the LRR-X microwave radiometer.

Keywords- radar, microwave radiometer, surface wind speed, rain rate, PR-2, LRR

I. INTRODUCTION:

Remote sensing of the vertical profile of precipitation and the near-surface wind speed over the ocean is important for the improvement of numerical weather and climate prediction, including the tracking of the global water cycle and release of latent heat, and increasing our understanding of cloud microphysical processes. Also, accurately measuring the wind field under heavy rain is important for hurricane research and improving forecast models. A retrieval algorithm has been developed which uses measurements of the backscattering coefficient from the PR-2 dual-frequency Doppler radar and horizontally polarized brightness temperature (T_B) measurements from the LRR-X 10.7 GHz radiometer to simultaneously retrieve the vertical profile of precipitation and the near-surface wind speed. Results are presented from a field campaign in June of 2003 in which several DC-8 overflights were made in regions of stratiform and convective precipitation associated with a mid-latitude cyclone off the coast of Vancouver, Canada.

The retrieval algorithm uses the radar backscatter measurements at each frequency to iteratively solve for two parameters of the gamma drop size distribution (GDSD) at each radar range gate. In light rain, the measured backscatter is corrected for attenuation using a Hitschfeld-Borden approach [1], [2]. In this way, the attenuation is corrected top-down, starting from the storm-top and progressing to the surface. The rain rate and liquid water content at each range gate can be determined by integrating the parameterized GDSDs. The surface wind speed is determined from the 10.7 GHz T_B by removing the atmospheric component and isolating the surface brightness, which is a function of wind speed. The atmospheric optical depth is determined by integrating the 10.7 GHz extinction coefficient determined at each rage gate using Mie theory with the parameterized GDSDs. The surface emissivity is then found by inverting the radiative transfer equation and using the integrated optical depth determined from the radar. A surface emissivity model is used to determine the near-surface wind speed. The top-down method becomes unstable in heavy rain; therefore a bottom-up approach is required.

With the bottom-up approach, the drop size distribution is parameterized starting with the range gate closest to the surface, then progresses upward towards the radar. This method requires an independently determined value for the total path integrated attenuation (PIA). This can be estimated from the radiometer provided that the wind speed is known. Since the wind speed is yet unknown, a simultaneous solution of DSD profile and wind speed is required.

II. INSTRUMENT DESCRIPTION

The instruments used in this study are the PR-2 Doppler radar, which operates at 13.4 and 35.6 GHz and the LRR-X 10.7 GHz horizontally polarized radiometer. The PR-2 mechanically scans cross-track to $\pm25^o$ and LRR-X electronically images cross-track to $\pm45^o$. The horizontal resolution of PR-2 is 800 m at the surface and LRR-X has a 500 m pixel resolution at the surface. The vertical resolution of PR-2 is 37 m. These instruments were deployed on a NASA DC-8 in June of 2003 at which time several overflights of precipitation were conducted.

III. METHODOLOGY

A. Light Rain – Top-down approach

The backscattering coefficient, $\sigma_b(f)$, of a rain volume is a function of the number distribution of drop sizes [3] and is given by

$$\sigma_b(f) = \int_{r_1}^{r_2} p(N_0, D_0, \mu, r)\xi_b(r, f)\pi r^2 dr, \qquad (1)$$

where $p(N_0, D_0, \mu, r)$ is the normalized gamma drop size distribution [4], $\zeta_b(r, f)$ is the Mie backscattering efficiency, r is the drop radius and f is the frequency. The gamma drop size distribution has three parameters which are an offset term N_0, a median drop diameter D_0, and a dispersion factor μ. Two parameters of the GDSD can be estimated given measurements of the backscattering coefficient at two frequencies. The μ and D_0 terms are estimated at each range gate using a Newton-Raphson least-squares iterative method with the 13.4 and 35.6 GHz backscatter measurements. It was observed that the iterative solution had the least error when N_0 was set to a constant and the μ and D_0 terms were solved for. An example of the retrieved μ and D_0 terms are shown in Fig. 1. In this profile, the melting layer starts at approximately 1500 m and is about 500 m thick. The median drop diameter increases in the melting layer due to smaller particles melting faster than the larger particles and exiting the layer with a faster velocity than the still melting larger particles. In the rain layer (below 1000 m), the median drop diameter and the dispersion factor increase towards the surface. This means that the width of the drop size distribution is becoming more narrow and the peak is moving toward a higher diameter closer to the surface. This is due to collisions and coalescence between the drops. Large drops will fall faster through the rain layer than the smaller drops and will collide and coalesce with the smaller drops in their path. This will cause the large drops to grow at the expense of the small drops, thus narrowing the DSD and moving the peak to a higher diameter.

The parameterized GDSD profile is used to determine the rain rate (RR), liquid water content (LWC), and the 10.7, 13.4, and 35.6 GHz extinction coefficients at each range bin. Fig. 2
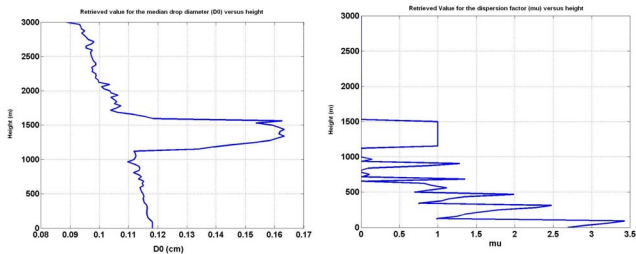
Figure 1. Retrieved profile of median drop diameter (left) and dispersion factor (right). The melting layer is around 1500 m and contains a peak of median drop diameters.
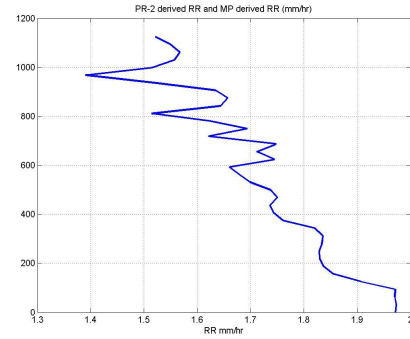
Figure 2. Retrieved rain rate profile from the parameterized DSD profile in Figure 1.

shows the retrieved rain rate profile in the rain layer for the same profile as in Fig. 1. The extinction coefficient at each level is determined from the parameterized GDSD using eqn. (1) with the Mie extinction efficiency, $\zeta ext(r, f)$, in place of the backscattering efficiency. The Maxwell-Garnett dielectric mixing model is used when determining the Mie efficiency of a particle with radius r in the frozen and melting layers [5]. In the frozen layer, the snow is assumed to be a mixture of air and ice with a density dependent upon the particle radius. In the melting layer, the particles are assumed to be a mixture of air, ice and water, where the concentrations of each are determined from a thermodynamic formula dependent on the height below the 273 K isotherm. The top and bottom height of the melting layer are determined using a bright-band detection algorithm adapted from [6]. The two way attenuation of the radar measurement is corrected by using the integrated 13.4 and 35.6 GHz extinction coefficients determined recursively from the storm top to the surface. In heavy rain, the top-down recursion becomes unstable and the profile must be solved starting from the surface and working towards the storm top using an independent estimate of the path integrated attenuation. This is discussed in section II.B.

To determine the surface wind speed, the surface emissivity is estimated by removing the atmospheric component from the measured 10.7 GHz T_Bs. A one layer radiative transfer equation is inverted using an effective atmospheric radiating temperature, determined from a coincident RaOb sounding, and the 10.7 GHz optical depth, which is determined by integrating the extinction coefficient profile associated with the parameterized GDSD profile. Fig. 3 shows the 10.7 GHz extinction coefficient profile. The extinction coefficient is observed to increase and peak in the melting layer then decrease to the lowest levels in the frozen layer. The level of the extinction coefficient in the melting layer as compared to the value in the rain layer is consistent with theoretical results [5]. Absorption from cloud liquid water and water vapor is included in this profile. The air is assumed saturated with vapor and the cloud liquid water is assumed constant at 0.2 mm. The cloud base was set to 600 m, which was the lifting condensation level determined from the RaOb sounding, and the cloud was assumed frozen above 1500 m. Once the surface emissivity is found for each LRR T_B measurement, the wind speed is estimated using the Pandey and Kakar [7] wind roughened ocean surface emission model with the Klein-Swift
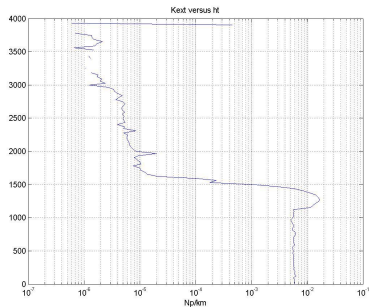
Figure 3. 10.7 GHz extinction coefficient versus height determined from the parameterzed GDSD in Figure 1. This profile is integrated to determine the optical depth associated with the measured LRR T_{BS}.

[8] dielectric model. The sea surface temperature was set to 284 K, which was measured by a buoy in the area.

B. Heavy Rain – Bottom-up approach

In heavy rain, the top-down attenuation correction becomes unstable and a bottom-up recursion is required. In this case, an independent estimate of the 13.4 and 35.6 GHz PIA is needed. The LRR T_B measurements can be used to determine the 10.7 GHz PIA for a given wind speed. An empirical formula derived from Mie theory is used to relate the 10.7 GHz PIA to the 13.4 and 35.6 GHz PIA. Fig. 4 shows the PIA versus wind speed at each frequency for an LRR T_B of 142.98 K. A bottom-up recursion is used with the PIA estimated at each wind speed and a simultaneous solution of wind speed and drop size distribution profile is found. The selected wind speed solution gives the lowest total RMS error between the measured/attenuation-corrected radar backscatter and the modeled backscatter from the iterative GDSD solution. This is illustrated in Fig. 5 for two rain rates.
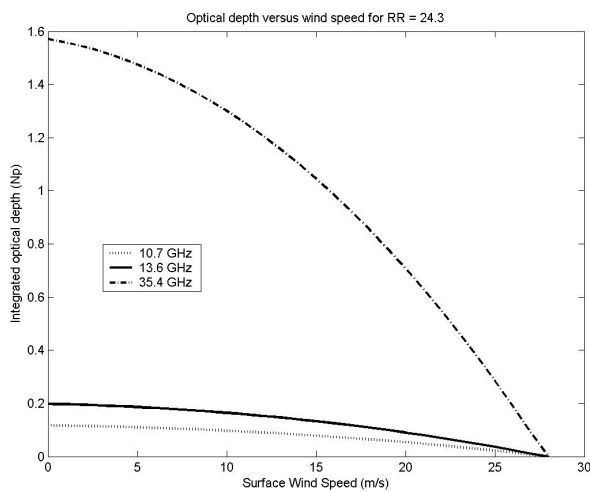
Figure 4. The 10.7 GHz PIA is estimated for each wind speed for a given T_B measurement. An empirical relation is used to estimate the 13.4 and 35.6 GHz PIA from the 10.7 GHz PIA.
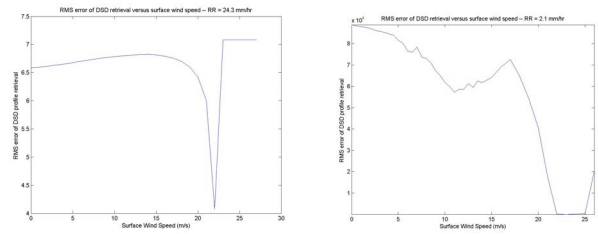
Figure 5. The RMS error of the GDSD iterative solution using the PIA estimate at each wind speed. The RR for the plot on the left is 24.3 mm/hr and 2.3 mm/hr for the plot on the right. The wind speed solution is 22 m/s for the left plot and 23 m/s for the right plot.

IV. RESULTS

The methods described in section III are used to create wind speed and rain rate images using the LRR and PR-2 data. Fig. 6 shows the vertical and cross track 13.4 GHz reflectivity measurements for an observed storm cell. Figure 7 shows the measured LRR brightness temperature for the same storm cell. The surface wind speed and rain rate were found and the results are shown in Fig. 8. The color image is the surface wind speed in m/s and contours of rain rate in mm/hr are overlayed. The rain rate values represent the average in the rain layer. Outflow from the storm is observed interacting with the environmental wind. The environmental wind is approximately 12 m/s blowing towards 17^0 from true north (NNE) as measured from a buoy at the time of the overflight. The outflow from the storm increases the wind field on the north side of the storm since the gust is blowing with the wind.
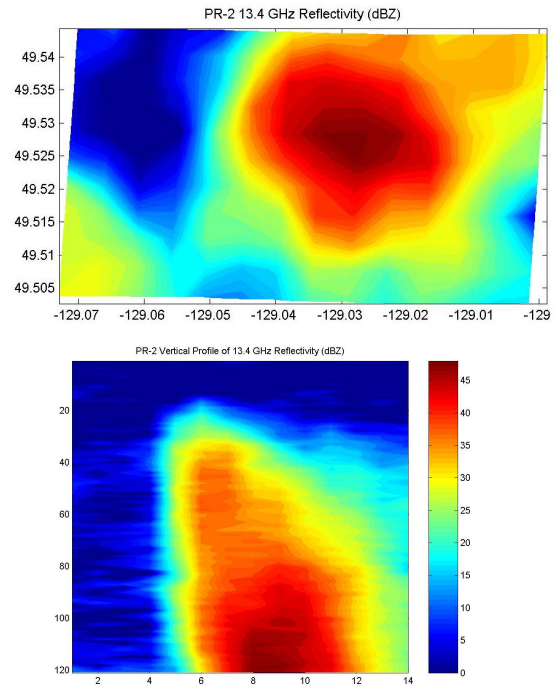
Figure 6. PR-2 reflectivity over a storm cell. The top image is a cross track view and the bottom image is a vertical profile through the center of the storm.

The outflow decreases the wind speed on the southern side of the storm because the gust is blowing into the environmental wind field. The center of the rain cell has rain rates of about 22 mm/hr. The maximum winds are around 26 m/s.

V. CONCLUSIONS

A retrieval algorithm is developed which uses dual-frequency radar backscatter and 10.7 GHz brightness temperature to remotely sense the surface wind speed and rain rate profile over the ocean. The radar backscatter is used to parameterize the gamma drop size distribution at each radar range gate. The attenuation of the radar backscatter is corrected using a top-down recursion in light rain and a bottom-up recursion in heavy rain.

The parameterized DSDs are used to determine the rain rate profile and the atmospheric contribution to the measured 10.7 GHz T_B. The surface contribution to the T_B is isolated by inverting the radiative transfer equation and removing the atmosphere. A wind roughed ocean surface emission model is used to determine the wind speed from the surface brightness. In heavy rain, a bottom-up recursion is used with an independent estimate of the attenuation at the radar frequencies. The attenuation is estimated from the radiometer as a function of wind speed, and a simultaneous solution of wind speed and DSD profile are found. Results of the retrieval algorithm applied to data from a field campaign are encouraging. A careful validation and error analysis of the wind and rain retrievals is currently in process.

VI. REFERENCES

[1] W. Hitschfeld and J. Bordan, "Errors inherent in the radar measurement of rainfall at attenuating wavelengths," *J. Atmos. Sci.*, vol. 11, pp. 58-67, 1954.

[2] R. Meneghini, H. Kumagai, J. Wang, T. Iguchi, T. Kozu, "Microphysical Retrievals over Stratiform Rain Using Measurements from an Airborne Dual-Wavelength Radar-Radiometer," *IEEE Trans. Geosci. Rem. Sens*, vol 35, no. 3, 1997.

[3] F. Ulaby, R. Moore, and A. Fung, Microwave Remote Sensing, Active and Passive. Volume I: Microwave Remote Sensing Fundamentals and Radiometry. Dedham, MA: Artech House, 1981, Ch. 5.

[4] N. Viltard, C. Kummerow, W. Olson, and Y. Hong, "Combined use of the radar and radiometer of TRMM to estimate the influence of drop size distribution on rain retrievals," *J. Applied Met.*, vol. 39, pp. 2103-2114, 2000.

[5] P. Bauer. J. Baptista, and M. Delulis, "The Effect of the Melting Layer on the Microwave Emission of Clouds over the Ocean*," J. Atmos. Sci.*, vol 56, pp 852-867, 1999

[6] W. Klaassen, "Radar observations and simulation of the melting layer of precipitation," *J. of Atmos. Sci.*, vol. 45, no. 24, 1988.

[7] P.C. Pandey and R.K. Kakar, "An Empirical Microwave Emissivity Model for a Foam-Covered Sea," *IEEE Journal of Oceanic Engin*, Vol OE-7, no. 3, 135-140, 1982

[8] L. A. Klein. and C. T. Swift, "An improved model for the dielectric constant of sea water at microwave frequencies," *IEEE Trans. Ant. Propogat*, vol 25, pp 104-111, 1976.
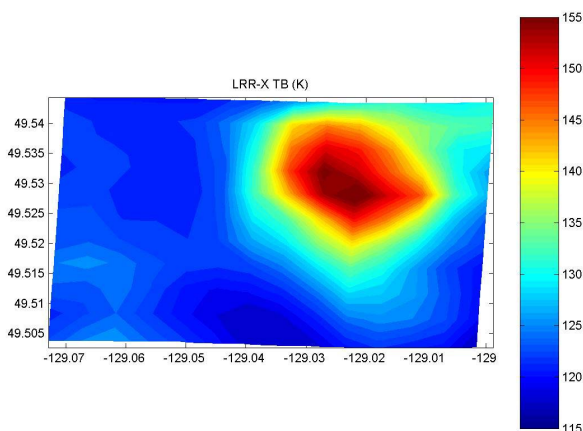
Figure 7. LRR-X T_B image over the same storm cell in Figure 6.
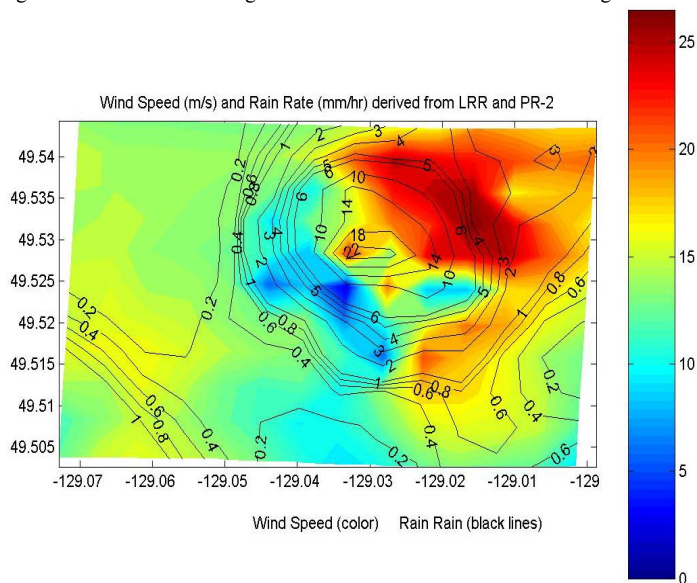
Figure 8. Wind speed and rain rate image over the storm cell shown in figures 6 and 7. Outflow from the storm is interacting with the environmental wind field which is blowing toward the NNE at 12 m/s.